Zeitschrift für Physikalische Chemie, Bd. 198, S. 73–85 (1997)

A Photoelectron Diffraction Study of the Pd{111}($\sqrt{3}\times\sqrt{3}$)R30°-CO Chemisorption Phase

By V. Fernandez, T. Gießel, O. Schaff, K.-M. Schindler, A. Theobald, C. J. Hirschmugl, S. Bao, A. M. Bradshaw

Fritz-Haber-Institut der Max-Planck-Gesellschaft,
Faradayweg 4–6, D-14195 Berlin-Dahlem, Germany

C. Baddeley, A. F. Lee, R. M. Lambert

Department of Chemistry, University of Cambridge,
Lensfield Road, Cambridge CB2 1EW, England

D. P. Woodruff

Department of Physics, University of Warwick, Coventry CV4 7AL, England

and V. Fritzsche

Institut für Theoretische Physik, Technische Universität Dresden,
D-01062 Dresden, Germany

Dedicated to Gerhard Ertl on the occasion of his 60th birthday

(Received May 6, 1996)

Adsorption / Electron scattering / Photoelectron spectroscopy / Single Crystals / Surface structure

Using scanned-energy mode photoelectron diffraction we show that in the Pd{111}($\sqrt{3}\times\sqrt{3}$)R30°-CO phase fcc hollow sites are occupied with a carbon-Pd layer spacing of 1.27 (±0.05) Å. This agrees very well with a relatively early LEED result of the Somorjai group and indicates that the experimental problems associated with applying scanned-energy mode photoelectron diffraction to second row transition metal substrates are not insurmountable.

Mittels energieabhängiger Photoelektronenbeugung wird gezeigt, daß CO in der Pd{111}($\sqrt{3}\times\sqrt{3}$)R30°-Phase in den fcc-Muldenplätzen mit einem Abstand von 1.27 (±0.05) Å relativ zur ersten Pd-Schicht adsorbiert. Dieses Ergebnis stimmt gut mit frühen LEED-Untersuchungen der Somorjai-Gruppe überein und zeigt ferner, daß die Photoelektronenbeugung auch bei Übergangsmetallen der zweiten Reihe Verwendung finden kann.

1. Introduction

Before the routine application of quantitative structural techniques the orientation and, in some cases, the binding site of adsorbed molecules were determined with vibrational spectroscopy, photoemission or near-edge X-ray absorption spectroscopy. Whereas many of the general conclusions drawn from these qualitative, or semiquantitative, studies have been shown to be essentially correct, some discrepancies have emerged. Thus, in the case of CO on Ni{111} vibrational spectra suggested that after initial adsorption in threefold symmetric hollow sites, bridge sites are occupied at higher coverages. In fact, adsorption continues to occur in hollow sites up to a coverage of 0.5 where the C−O stretching frequency has a value of 1905 cm^{-1} [1]. Moreover co-adsorption of CO with oxygen on the same surface produces a sharp band at 2099 cm^{-1} indicative perhaps of CO in an atop site, although a recent quantitative structural analysis again shows that the CO remains in hollow sites [2]. A similar discrepancy exists for Pd{110}-CO where the C−O stretch indicates a bridge site, but the atop site appears to be occupied [3]. In a further example, near-edge X-ray absorption spectra have indicated that the surface methoxy species is tilted by as much as 30° relative to the normal on copper surfaces, whereas quantitative structural studies on Cu{111} and Ni{111} show that the O-C axis is perpendicular to the surface [4]. Again, in the case of ethene adsorption, recent photoelectron diffraction [5] and STM [6] studies of the system Cu{110}-C_2H_4 have also shown that the short bridge site is occupied with the C-C axis parallel to the surface and oriented in the ⟨110⟩ azimuth, a result which is at variance with earlier IR work.

This situation emphasises the need to produce a more extensive data base for the structure of molecules on metal surfaces. In the case of carbon monoxide adsorption several quantitative studies have appeared in the last few years, mostly with low energy electron diffraction (LEED), but also with photoelectron diffraction. The latter technique has distinct advantages over LEED when the adsorbed layer in question shows little or no long-range order or when it is particularly susceptible to electron beam damage. CO adsorption on Cu{110} [7] is an example of a system which has both these properties. Photoelectron diffraction in the scanned energy mode [8, 9] involves the measurement of an adsorbate core-level photoelectron line at a pre-selected emission angle as a function of photon energy, and thus of photoelectron energy. (Clearly, synchrotron radiation is required for this experiment, since conventional soft X-ray sources for photoelectron spectroscopy have a fixed photon energy). The dependence of photoelectron intensity on kinetic energy is modulated by the interference between the directly emitted component of the photoelectron wave and the components that arise from elastic scattering at the neighbouring substrate atoms. The modulations depend in turn on the respective path length differences and

thus provide information on the local geometry of the emitter atom. The latter is extracted in a similar way to LEED by comparing experimental "modulation functions" with simulated curves calculated using multiple scattering theory.

Photoelectron diffraction is also particularly well suited to investigate the adsorption of CO on Pd{111}-CO which was one of the first systems studied by Ertl and coworkers in the 1970's [10]. It displays an especially complicated series of ordered structures (at least seventeen!) [11, 12], many of which have very large unit cells (e.g. ($\sqrt{3}\times 35$)rect at $\theta = 0.514$) and are thus not readily accessible with LEED I-V analysis. On the other hand, the corresponding vibrational spectra, together with the LEED patterns, suggest that there is only a small number of different local geometries for the CO molecule throughout the adsorption sequence. Of additional interest is the $c(4\times 2)$, or ($\sqrt{3}\times\sqrt{2}$)rect, structure formed at $\theta = 0.5$ in an analogous way to that on Ni{111} described above. Previous assignments of the vibrational spectrum at this coverage have also placed the CO molecules on bridge sites [11, 13, 14], which in the case of the Ni system has subsequently proved to be incorrect. It is clear that a quantitative structural study of the Pd system at various coverages is now necessary. Our previous photoelectron diffraction studies have been restricted, however, to first row transition metal surfaces because of complications in the data analysis caused by Auger electron emission. In the case of Pd, for example, the kinetic energy range between 100 and 350 eV is characterised by the strong substrate MNN Auger lines of constant energy upon which the photoelectron lines (of variable energy) are superimposed. This causes substantial problems in the integration of the raw data, as will be illustrated below. For this reason, the present preliminary study has been restricted to the ($\sqrt{3}\times\sqrt{3}$)R30°, or $c(\sqrt{3}\times\sqrt{3})$rect, structure at $\theta = 0.33$ which has already been the subject of a relatively early LEED analysis [15]. Our results show that it is indeed possible to analyse photoelectron diffraction data in such a situation and that the structural parameters obtained for this system agree extremely well with the previous LEED study.

2. Experimental details, data analysis and simulations

The experiments were performed in a purpose-built ultra-high vacuum system on the HE-TGM-1 monochromator [16] at the BESSY synchrotron radiation source. A 152 mm mean radius 150° electrostatic deflection analyser with three parallel channeltrons (VG Scientific) was used to measure the photoelectron diffraction signal at a fixed angle of 60° relative to the photon incidence direction. The Pd{111} sample was prepared by the usual methods of orientation with Laue X-ray diffraction, spark machining, polishing and in-situ cleaning with argon bombardment and anneal cycles.

In order to completely remove carbon it was found necessary to perform occasional oxygen treatments (300 s at 5×10^{-8} mbar and 850 K). After such a treatment a well defined (1×1) LEED pattern was observed. The atomic cleanliness was monitored with photoelectron spectroscopy using synchrotron radiation. The C 1*s* photoelectron diffraction spectra were taken at polar angles between 0 and 60°, in steps of 10°, in all three principle azimuths. The signal was recorded at successive photon energies (separated by 2 eV) for kinetic energies of about ±20 eV around the C 1*s* core level peak to give the energy distribution curves (EDC's). The intensity of each of these peaks was then determined by background subtraction and integration, and the resulting intensity-energy spectra were normalised to give the modulation functions [17]. Unfortunately, it is not possible at present to measure the corresponding O 1*s* modulation functions because the O 1*s* photoelectron line has almost the same binding energy as the Pd $3p_{3/2}$ feature at 532 eV. Future measurements at higher resolution on third generation synchrotron radiation sources may eliminate this problem.

The particular problems encountered with palladium as substrate are illustrated in Fig. 1 which shows the C 1*s* photoelectron line of CO adsorbed on (a) Ni{111} and (b) Pd{111} plotted successively in steps of 2 eV photon energy on a kinetic energy scale. The inset in Fig. 1a is an expanded-scale view of the range 460−520 eV and illustrates this principle more clearly. Immediately obvious in this plot are the modulations in the height of the peak due to the photoelectron diffraction effect; these are seen more clearly in the corresponding modulation function after integration and normalisation (Fig. 2a). Three prominent features are also observed in the background and have intensities comparable to that of the modulations. The feature at about 50 eV is due to the Ni MNN Auger transition. The features at ~270 eV and ~500 eV derive from the C KLL and O KLL transitions associated with the CO molecule itself. The integration is somewhat more difficult in these energy regions, but does not prove to be a particularly serious problem, as Fig. 2a shows. In the case of Pd, however, the problems are at first sight insurmountable: the MNN Auger transitions are at least a factor of ten stronger than the intensity modulations, as can be seen in Fig. 1b. The fact that we have been able to analyse the data and obtain modulation functions that appear quite reasonable (Fig. 2b) is due to the development of new integration routines. These involve fitting each EDC with Gaussian function, a Gaussian-broadened step function and a background template. The latter is obtained from the overlapping high energy ends of the EDC's. The intensity is then taken as the area under the Gaussian function. Note that the modulations are actually almost a factor of 2 stronger than those for the Ni surface.

Quantitative structure determination proceeded in two stages [17]. A *direct method* was used to determine the adsorption site employing the full set of data (this is not actually necessary: fewer modulation functions can

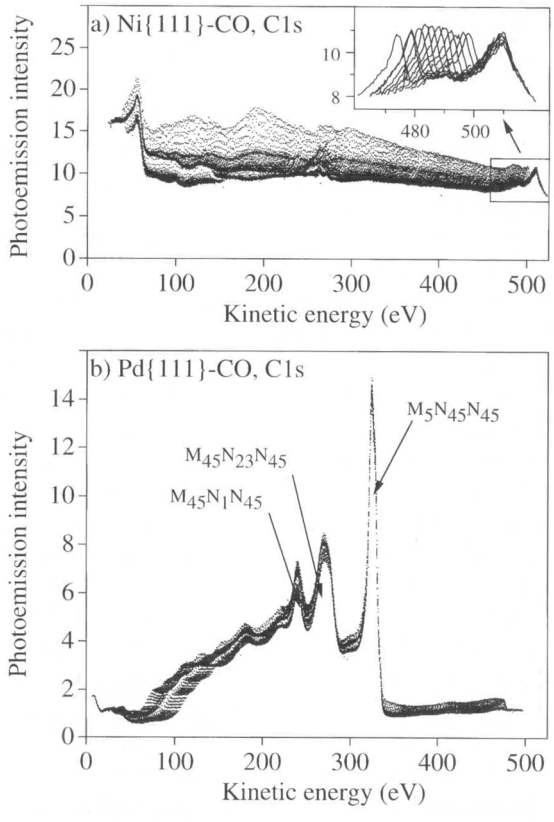

Fig. 1. Raw C 1*s* photoelectron diffraction data for (a) Ni{111}-CO and (b) Pd{111}-CO.

also be used) and calculating the "projection integrals" [18]. The underlying physical principle is that modulation functions recorded in directions which correspond to 180° scattering from a near-neighbour substrate atom ("the backscattering geometry") are typically dominated by this event and show particularly strong modulations [8, 9], which in turn leads to a high value of the projection integral. The result of this method is a threedimensional intensity map of the space around the emitter, with maximum amplitudes in regions corresponding to the nearest neighbour backscatterers. The second stage is a full quantitative structural analysis using an iterative "trial-and-error" procedure which involves a comparison of the experimental spectra with the results of multiple scattering simultations based on trial model structures. These calculations have been performed on the basis of an expansion of the final state wavefunction into a summation over all scattering pathways which the electron can take from the emitter atom to the detector

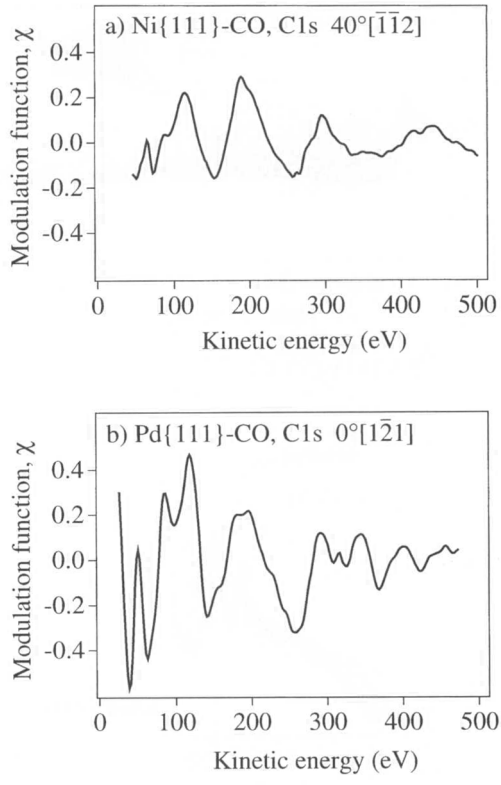

Fig. 2. Modulation functions derived from Figs. 1a and b, respectively.

outside the sample. A magnetic quantum number expansion has been used to calculate the scattering contribution of an individual scattering path [19]. Double and higher order scattering events were treated by means of the Reduced Angular Momentum Expansion (RAME) [20]. The finite energy resolution and angular acceptance of the electron analyzer are included. Anisotropic vibrations for the emitter atom and isotropic vibrations for the scattering atoms are also taken into account. The comparison between theory and experiment is aided by the use of a reliability factor $R_m = \Sigma (\chi_{th} - \chi_{ex})^2 / \Sigma (\chi_{th}^2 + \chi_{ex}^2)$, where a value of 0 corresponds to perfect agreement, a value of 1 to uncorrelated data, and a value of 2 to anticorrelated data [17].

3. Results and discussion

Fig. 3 shows the result of the application of the projection method to the complete data set for the Pd{111}($\sqrt{3} \times \sqrt{3}$)R30°-CO phase. As described

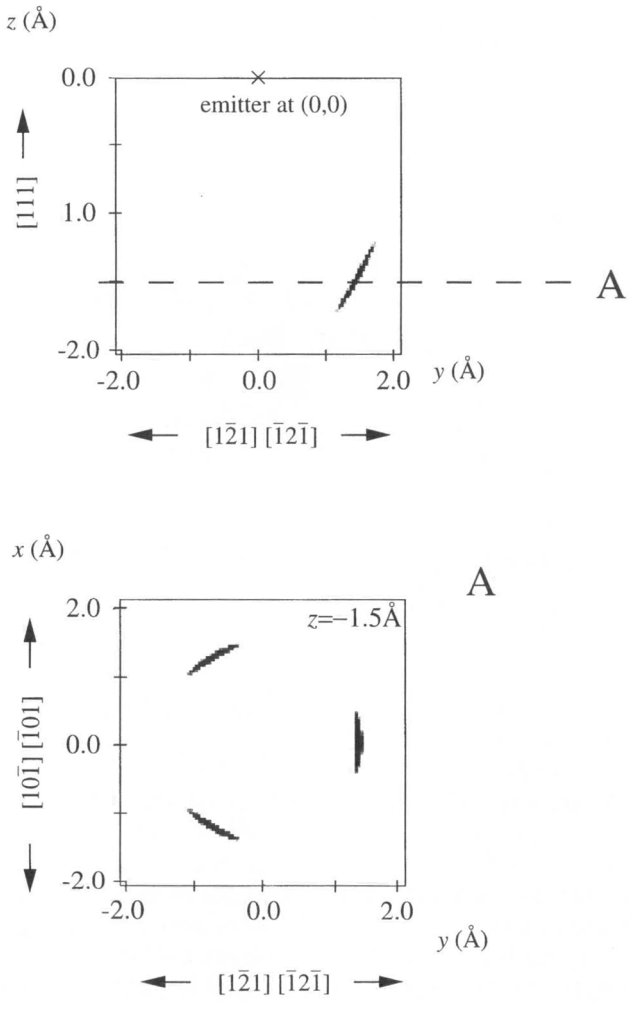

Fig. 3. Image of the nearest-neighbour substrate scatterers for the Pd{111}($\sqrt{3}\times\sqrt{3}$)-CO phase obtained by application of the projection method to the C 1*s* spectra. In the top panel the cut is perpendicular to the surface passing through the emitter; the bottom panel shows a cut parallel to the surface but at 1.5 Å below the emitter.

in the last Section, such grey-scale plots can be regarded as images of the nearest-neighbour substrate atoms [18]. Two cuts through a cube in real space directly "below" the emitting atom are shown. In the top panel the cut is perpendicular to the surface through the emitter in a ⟨211⟩ azimuth; in the bottom panel the cut is parallel to the surface, but 1.5 Å below the emitter. From the threefold rotational symmetry of the pattern and the sepa-

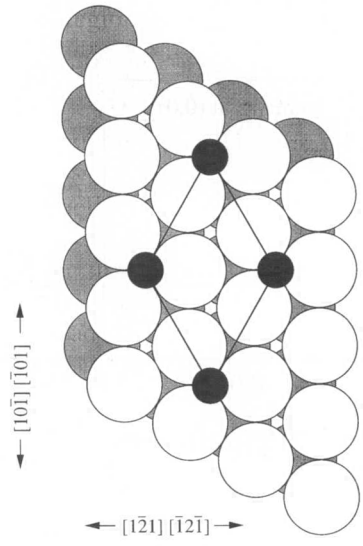

Fig. 4. Plan view of the Pd{111}($\sqrt{3}\times\sqrt{3}$)-CO structure.

ration between the emitter and the three features, it is immediately clear that the carbon atom, and thus the CO molecule, occupy a hollow site. Furthermore, from the azimuthal orientation of the threefold pattern relative to the known azimuthal orientation of the crystal during the measurements it can be ascertained that the so-called fcc hollow site is occupied. The latter is the hollow site with a Pd atom directly beneath in the third layer as opposed to that with a Pd atom directly beneath in the second layer ("hcp" site). This agrees completely with the determination in the LEED study of Ohtani *et al.* [15]. The ($\sqrt{3}\times\sqrt{3}$)R30° layer with the CO in this site is drawn schematically in Fig. 4, such that it can be directly compared with the bottom panel of Fig. 3.

Having established the surface site and the approximate vertical distance of the emitter above the outermost Pd layer, we can now perform the quantitative structural analysis using the trial-and-error scheme, but in a much reduced parameter space. The C 1*s* modulation functions for the eight different emission directions used in the analysis are shown as bold curves in Fig. 5. (Note that there is still some remnant of the strongest Auger feature just above 300 eV in most of the curves). The parameters varied are the C-Pd vertical layer spacing, z_{C1}, as well as the lateral displacements of the carbon atom and the three Pd atoms forming the adsorption site, Δr_C and Δr_{Pd}, respectively (Fig. 6). Since the present structural determination has somewhat preliminary – even exploratory – character (see Introduc-

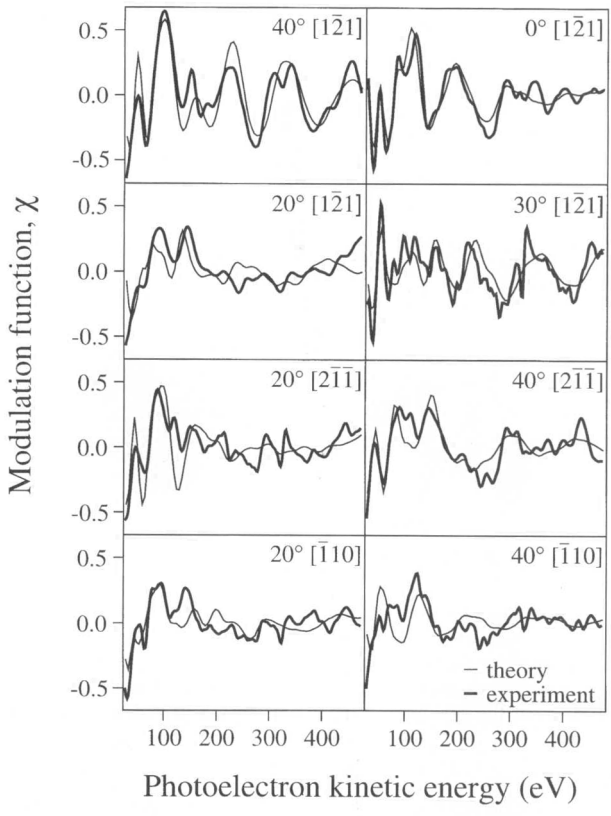

Fig. 5. Experimental C 1*s* modulation functions used in the multiple scattering structural optimisation compared with the results of the calculation for the best-fit structures as given in Table 1.

tion), certain parameters which are relatively ineffective in reducing the *R*-factor were not varied. The first Pd-Pd layer separation, for instance, was maintained at the bulk value of 2.25 Å.

The best fit is obtained for the values of the three parameters given in Table 1. The corresponding calculated modulation functions are shown in Fig. 5. The overall eight-spectrum *R*-factor is $R_m = 0.24$; the *R*-factors for the individual spectra are 0.14, 0.14, 0.37, 0.25, 0.36, 0.20, 0.31 and 0.57 for the 40°, 0°, 20° and 30° polar angles in the [1$\bar{2}$1] azimuth, 20° and 40° in the [2$\bar{1}\bar{1}$] azimuth and 20° and 40° in the [$\bar{1}$10] azimuth, respectively. Note that the best agreement between theory and experiment is obtained for normal emission and for the favoured back-scattering geometry (i.e. 40° in [1$\bar{2}$1]) in which there is a Pd substrate atom directly "behind" the emitter. This leads to a dominant single oscillation in the modulation function and

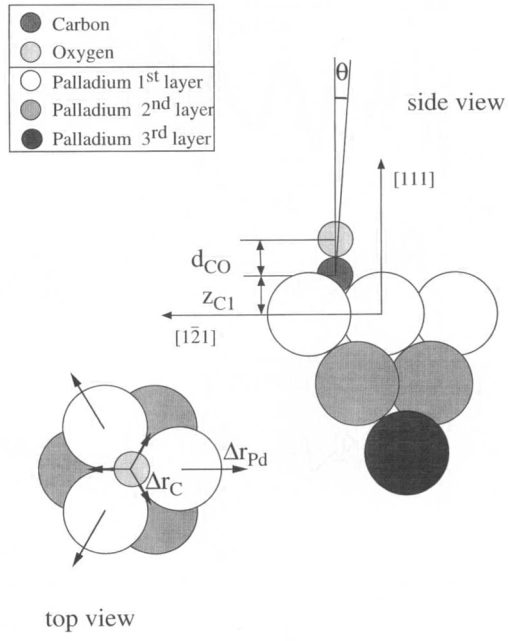

Fig. 6. Side and plan view of the structure of Pd{111}($\sqrt{3}\times\sqrt{3}$)-CO with the definition of the structural parameters used in the fitting procedure. The arrows in the plan view define the directions of the positive diplacements of the parameters Δr_{Pd} and Δr_C.

Table 1. Optimised values of the position parameters.

Parameter	Optimum value (present work)	Optimum value Ohtani *et al.* [15]
z_{C1}	1.27 (±0.05) Å	1.29 (±0.05) Å
Δr_{Pd}	0.00 (±0.10) Å	0.00 Å
Δr_C	0.01 (±0.10) Å	
d_{PdC}	2.03 (±0.04) Å	2.05 (±0.04) Å

good agreement between the experimental and simulated curves. The carbon-Pd layer separation of z_{C1} = 1.27 (±0.05) Å agrees very well with the LEED value of 1.29 (±0.05) Å [15]. Δr_{Pd} and Δr_C are, as expected, essentially zero, although the error bars here are ±0.10 Å. Fig. 7 shows the dependence of the *R*-factor on the three parameters and enables the errors to be calculated from the variance. Δr_C is an important parameter, because

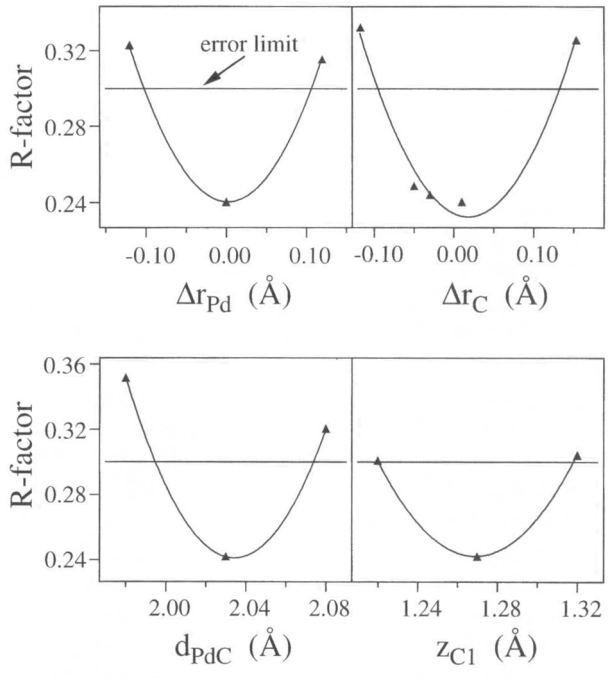

Fig. 7. Dependence of the multispectral *R*-factor on the values of each strutural parameter.

in the more complicated structures obtained at higher coverages it is necessary to consider not only the bridge sites but also the sites along the line between bridge and hollow.

The parameter to which the method is most sensitive is the nearest-neighbour distance, d_{PdC}. Its value and associated precision are 2.03 Å (±0.04); the dependence of the *R*-factor is also shown in Fig. 7. Not given in Table 1 are the values of d_{CO} = 1.25 (+0.14/−0.11) Å and θ = 0 (±23)° for the C−O bond length and the C−O tilt angle, respectively, since these can only be determined approximately from the C 1*s* data set. The scattering from the oxygen atom is much weaker than that from the Pd substrate and essentially in the forward direction. Normally, the combination of O 1*s* and C 1*s* data sets would give these parameters relatively accurately, e.g. [21]; as noted above, however, it has so far not been possible to measure the corresponding O 1*s* modulation functions.

In the zero coverage limit on Pd{111} the C−O stretching frequency occurs at 1807 cm^{-1}, shifting to 1848 cm^{-1} in the ($\sqrt{3}\times\sqrt{3}$)R30°, or ($\sqrt{3}\times$)rect, phase [11−13]. In the earliest IR study of this system it was concluded (correctly, as it transpires) that a hollow site is occupied [13]. The transition to the $c(4\times2)$, or ($\sqrt{3}\times2$)rect, structure at θ = 0.5 occurs

via a series of ordered overlayers which may be designated $(\sqrt{3}\times n)$rect or $c(\sqrt{3}\times n)$rect where n is an odd integer. Six have been identified [12] but more could possibly be observed at lower temperature [11]. At the same time, the C–O stretch shifts to 1920 cm^{-1} [corresponding to the $c(4\times2)$ structure] via a series of spectra containing up to three different bands. Bradshaw and Hoffmann [13], as well as later authors, interpreted this shift in terms of a switching to bridge sites, although an equally possible explanation on the basis of the LEED pattern alone would be further adsorption of CO in hollow sites. This would then lead to the formation of a $c(4\times2)$ structure in which equal numbers of fcc and hcp hollow sites are occupied, as in the case of CO and Ni{111}. We have already recorded the corresponding photoelectron diffraction data for the $c(4\times2)$ structure and are currently analysing them. (The structure is actually somewhat unstable and changes readily into one of higher or lower coverage, implying that it occupies only a very narrow range in the θ-T phase diagram). The first results suggest that the hcp and fcc hollow sites are occupied.

Finally, we note that in the corresponding system Ni{111}-CO no $(\sqrt{3}\times\sqrt{3})$R30° structure is formed at $\theta = 0.33$ [22], although a (2×2) structure at $\theta \sim 0.25$ has recently been reported [23]. In the latter, a mixture of fcc and hcp hollow sites are occupied with z_{C1} (hcp) = 1.26 (±0.04) Å, z_{C1} (fcc) = 1.30 (±0.08) Å and percent hcp sites = 64 (±22)%. The error bars on the layer spacings both in these and the present data are thus too large to make any meaningful comparison of bond lengths. The vibrational frequency at $\theta \sim 0.33$ in the Ni{111}-CO system is somewhat higher at ~1880 cm^{-1} [22] compared to 1848 cm^{-1} in Pd{111}-CO. It is also not possible to measure at present the other interesting structural parameter, d_{CO}, with the necessary accuracy for comparative studies, even if the O 1*s* modulation functions are available [21]. This also applies to the quantitative LEED investigations where d_{CO} is also typically given with an error bar of ±0.05 Å.

4. Conclusions

The present results indicate that it is indeed possible to perform scanned energy mode photoelectron diffraction on surfaces of the second row transition metals. Despite the strong substrate MNN Auger electron emission which gives rise to an intense and strongly varying background to the adsorbate photoelectron line, it proves possible to extract the diffraction data. In this first example we confirm that CO adsorbed on Pd{111} in the $(\sqrt{3}\times\sqrt{3})$R30° phase takes up fcc hollow sites with a carbon-Pd layer separation of 1.27 (±0.05) Å. This result is in excellent agreement with a relatively early LEED study.

Acknowledgements

This work has been supported financially by the German Federal Ministry of Research and Technology (BMFT) under contract number 05 5EBFXB 2, the British Science and Engineering Research Council (SERC) and the EU Human Capital and Mobility and Large Scale Installation programmes.

References

1. K.-M. Schindler, Ph., Hofmann, K. U. Weiss, R. Dippel, P. Gardner, V. Fritzsche, A. M. Bradshaw, D. P. Woodruff, M. E. Davila, M. C. Asensio, J. C. Conesa and A. R. Gonzalez-Elipez, J. Electron Spectrosc. Relat. Phenom. **64/65** (1993) 75.
2. V. Fernandez, K.-M. Schindler, O. Schaff, Ph. Hofmann, A. Theobald, A. M. Bradshaw, V. Fritzsche, R. Davis and D. P. Woodruff, Surf. Sci. **351** (1996) 1.
3. A. Wander, P. Hu and D. A. King, Chem. Phys. Lett. **201** (1993) 393.
4. O. Schaff, G. Hess, V. Fernandez, K.-M. Schindler, A. Theobald, Ph. Hofmann, A. M. Bradshaw, V. Fritzsche, R. Davis and D. P. Woodruff, J. Electron Spectrosc. Relat. Phenom. **75** (1995) 117.
5. O. Schaff, V. Fernandez, Ph. Hofmann, K.-M. Schindler, A. Theobald, V. Fritzsche, A. M. Bradshaw, R. Davis and D. P. Woodruff, Surf. Sci. **348** (1996) 89.
6. J. Buisset, H. P. Rust, E. Schweizer, L. Cramer and A. M. Bradshaw, Phys. Rev. B, in press.
7. Ph. Hofmann, K.-M. Schindler, S. Bao, V. Fritzsche, A. M. Bradshaw and D. P. Woodruff, Surf. Sci. **337** (1995) 169.
8. D. P. Woodruff and A. M. Bradshaw, Rep. Prog. Phys. **57** (1994) 1029.
9. A. M. Bradshaw and D. P. Woodruff, in: "*Applications of synchrotron radiation: High Resolution Studies of Molecules and Molecular Adsorbates on Surfaces*", ed. W. Eberhardt, Springer, Berlin (1995) p. 127.
10. G. Ertl and J. Koch, Z. Naturforschung **25a** (1970) 1906; H. Conrad, G. Ertl and J. Küppers, Surf. Sci. **76** (1978) 323.
11. M. Tüshaus, W. Berndt, H. Conrad, A. M. Bradshaw and B. Persson, Appl. Phys. **A51** (1990) 91.
12. W. Berndt, M. Tüshaus, D. Hoge and A. M. Bradshaw, to be published.
13. A. M. Bradshaw and F. M. Hoffmann, Surf. Sci **72** (1978) 513.
14. W. K. Kuhn, J. Szanyi and D. W. Goodman, Surf. Sci. **274** (1992) L611; J. Szanyi, W. K. Kuhn and D. W. Goodman, J. Vac. Sci. Technol. **A11** (1993) 1969.
15. H. Ohtani, M. A. Van Hove and G. A. Somorjai, Surf. Sci. **187** (1987) 372.
16. E. Dietz, W. Braun, A. M. Bradshaw and R. L. Johnson, Nucl. Instrum. Meths. **A239** (1985) 359.
17. Ph. Hofmann, K.-M. Schindler, S. Bao, V. Fritzsche, A. M. Bradshaw and D. P. Woodruff, Surf. Sci. **337** (1995) 169.
18. Ph. Hofmann and K.-M. Schindler, Phys. Rev. B **47** (1993) 13941; Ph. Hofmann, K.-M. Schindler, S. Bao, A. M. Bradshaw and D. P. Woodruff, Nature **368** (1994) 131.
19. V. Fritzsche, J. Phys. Condens, Matter **2** (1990) 1413; Surf. Sci. **265** (1992) 187.
20. V. Fritzsche, Surf. Sci. **213** (1998) 648.
21. R. Davis, D. P. Woodruff, O. Schaff, V. Fernandez, K.-M. Schindler, Ph. Hofmann, K.-U. Weiss, R. Dippel, V. Fritzsche and A. M. Bradshaw, Phys. Rev. Lett. **74** (1995) 1621.
22. L. Surnev, Z. Xu and J. T. Yates, Jr., Surf. Sci. **201** (1988) 1.
23. R. Davis, D. P. Woodruff, Ph. Hofmann, O. Schaff, V. Fernandez, K.-M. Schindler, V. Fritzsche and A. M. Bradshaw, J. Phys.: Condens. Matter **8** (1996) 1367.